Biomechanical and Bone Histomorphological Evaluation of Two Surfaces on Tapered and Cylindrical Root Form Implants: An Experimental Study in Dogs

Bruno Negri, DDS, PhD;* José Luis Calvo-Guirado, DDS, PhD, MS;†
José Eduardo Maté Sánchez de Val, DDS, PhD, MS;‡ Rafael Arcesio Delgado Ruiz, DDS, PhD, MS;‡
María Piedad Ramírez Fernández, DDS, PhD, MS;* Gerardo Gómez Moreno, DDS, PhD, MS;§
Antonio Aguilar Salvatierra, DDS, PhD;* Javier Guardia, DDS, PhD, MS;*
Fernando Muñoz Guzón, DDS, PhD, MS¶

ABSTRACT

Purpose: The aim of this study was to evaluate the early bone response of tapered and cylindrical root form implants with two different surface treatments in fresh extraction sockets after 4 and 8 weeks.

Materials and Methods: Surface treatments and implant design comprised ($n = 9$ each): tapered with dual acid-etched surface; tapered with dual acid-etched and sandblasted surface (T DAE SB); cylindrical with dual acid-etched surface (C DAE); and cylindrical with dual acid-etched and sandblasted surface (C DAE SB). Implants were placed in the distal sockets of mandibular premolars (${}_2P_2, {}_3P_3, {}_4P_4$) of six beagle dogs, remaining in vivo for 4 and 8 weeks. After sacrifice, the implants were subjected to torque to the point of interface fracture and subsequently nondecalcified for histomorphological study. Statistical analysis was performed by a General Linear Model (GLM) analysis of variance model with a significance level of 5%.

Results: Torque to interface fracture was significantly greater for the C DAE SB group than for the other groups ($p < .001$). Histomorphological analysis showed woven bone formation around all implant surfaces at 4 weeks and its replacement by lamellar bone at 8 weeks. Study time (4 or 8 weeks) did not affect torque measures.

Conclusions: The double acid-etched and sandblasted sample surface increased early bone biomechanical fixation of both cylindrical and tapered root form implants. The cylindrical root form implants showed higher torque to interface fracture values when compared with the tapered root form implants. The C DAE SB surface group showed the highest biomechanical fixation values ($p < .001$).

KEY WORDS: animal model, cylindrical design, dual acid etched, sandblasted, tapered design

INTRODUCTION

The use of endosseous implants in jaws has become one of the most successful treatment modalities in dentistry, with frequent reports of success rates of greater than 90%.[1,2] However, in spite of these high success rates, researchers and clinicians have attempted to decrease treatment time frames by reducing the healing period during which osseointegration is established.[3] The most common approach to this objective is through modification of implant design parameters.[4]

Implant design alterations have included changes to its structural material,[5,6] to macrogeometry and/or surgical instrumentation,[7–9] and/or surface

*Collaborator professor of Master in Implant Dentistry, Faculty of Medicine and Dentistry, University of Murcia, Murcia, Spain; †senior lecturer in General and Implant Dentistry, Faculty of Medicine and Dentistry, University of Murcia, Murcia, Spain; ‡associate professor in Restorative Dentistry, Faculty of Medicine and Dentistry, University of Murcia, Murcia, Spain; §senior lecturer of Farmacological Interactions, Faculty of Dentristry, University of Granada, Granada, Spain; ¶lecturer in General Veterinary, Faculty of Veterinary, University of Santiago de Compostela, Lugo, Spain

Reprint requests: Dr. Bruno Negri, Faculty of Medicine and Dentistry, University of Murcia, C/Carretillas 25, 1° 8, Pilar de la Horadada, Alicante 03190, Spain; e-mail: stonefly50@hotmail.com

DOI 10.1111/j.1708-8208.2011.00431.x

modifications.[3,4,10,11] Although it has not been clearly established whether or not biocompatible materials other than titanium and its alloys improve the host-to-implant response, alterations to macrogeometry and/or surgical instrumentation and/or surface modifications have been found to produce significant effects during the early stages of bone healing around endosseous implants.[3,4,7–13]

Regarding implant macrodesign and surgical instrumentation, research has identified two basic different bone healing issues that lead to implant integration with the bone tissue.[7–13] The first is when an intimate surgical fit between bone and the implant's screw root form results in the formation of blood clots in the region between bone and implant surface, which is subsequently substituted by new bone.[14] The second is when healing chambers develop due to the interplay between implant design and drilling dimensions, leading to an intramembranous-like woven bone formation in large void spaces occupied by blood clots immediately after implantation.[7–9] Whatever the healing pathway, histomorphometric studies have shown that integration rates are similar during early healing stages[9–13] and that long-term stability is assured by bone modeling and remodeling processes.[14]

Dental implants transfer load to surrounding biological tissues. In this way, the primary functional design objective is to manage (dissipate and distribute) biomechanical loads. Implant thread configuration is an important factor for the biomechanical optimization of implant design. For this reason, biomechanical concepts and principles must be applied to the implant's thread design in order to enhance clinical success.[13] Thread geometry involves thread pitch, depth, and shape. Although thread pitch and depth may affect stress distribution, manufacturers have traditionally provided implant systems of a constant pitch and depth. So, for commercial implant system design, the main issue is one of modification to thread configuration. Threads are designed to maximize initial contact, augment surface area, and facilitate the dissipation of stresses at the bone-to-implant interface.[13]

Among these alterations to implant design, surface modification has been by far the most widely researched factor.[3,4,10,11] In light of this research, mass-produced implant surface design has shifted from as-turned to moderately rough (i.e., dual acid etched, grit blasted, sandblasted, or anodized), and these modifications have shown positive early healing modulation and higher biomechanical fixation.[3,4,10,11,15–18] Chemical modifications, such as the incorporation of hydroxyapatite as a surface coating by means of a variety of processes, have also led to highly osteoconductive surfaces.[19] However, weak interfaces between the surface coating and implant substrate, such as those found in plasma-sprayed hydroxyapatite (PSHA), have raised concerns regarding their long-term clinical performance.[19] Recently, the combination of surface roughness and the incorporation of bioceramics in the nanometer (or elemental chemistry) length scales has shown promising results compared with moderately rough surfaces in scenarios both with and without healing chamber development around implants.[4,12,19–26]

The objective of the present study was to evaluate early bone responses (biomechanical fixation and histomorphology) to tapered and cylindrical implants treated with two different surface treatments.

MATERIALS AND METHODS

The Ethics Committee for Animal Research at the University of Murcia, Spain approved the study protocol that followed guidelines established by the European Union Council Directive of November 24th, 1986 (86/609/EEC).

Six male beagle dogs, 1.5 years in age, weighing approximately 14–15 kg, and in good health, were used in the study. The animals were split into two groups of three animals each for evaluation at 4 and 8 weeks. All animals presented intact maxillas, without any general occlusal trauma or oral viral or fungal lesions. Clinical examination determined that the dogs were in good general health, with no systemic involvement.

Implants

This study used tapered and cylindrical endosseous Ti-6Al-4V implants of 3.75 mm diameter and 10 mm length (Figure 1, A and B). These implant groups were subdivided according to surface treatment as follows: tapered with dual acid-etched surfaces (T DAE); tapered with dual acid-etched and sandblasted surfaces (T DAE SB); cylindrical with dual acid-etched surfaces (C DAE); cylindrical with dual acid-etched and sandblasted surfaces (C DAE SB) (B and W S.R.L., Buenos Aires, Argentina) (see Figure 1, C and D). There were nine samples in each group ($n = 9$).

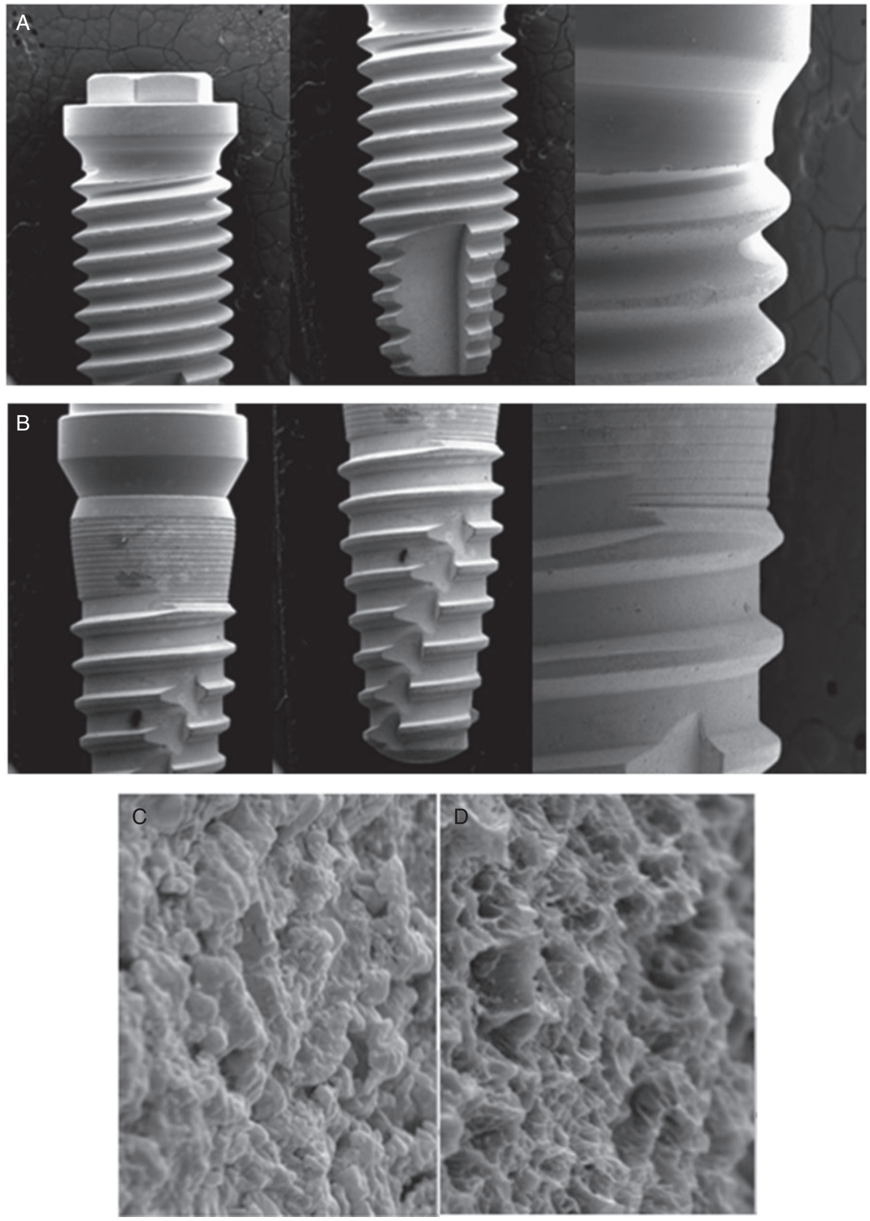

Figure 1 *A*, Cylindrical design, ×12 and ×25 magnification. *B*, Tapered design, ×12 and ×25 magnification. *C* and *D*, Double acid-etched surface (C); Double acid-etched/sand blasted surface (D). Note the different topograghy ×6,000 magnification.

The pitch distance was 0.4 mm for the cylindrical implants and 0.8 mm for the tapered implants. The implants underwent a microstructured subtractive surface treatment through the double acid-etching and sandblasting processes.

The double acid-etching process was performed by immersing the implant in a H_2SO_4 solution for 72 hours followed by Hydrochloric Acid (HCl) solution for 30-hour period. The surface produced had micropits of 1–6 µm and valleys of 10–15 µm. Mean Sa values ranged between 2.08 µm and 2.24 µm, while the sandblasting technique was performed by Silica grit of 250–500 µm, which results in macroroughness patter with valleys of 30–50 µm and was then followed by dual acid etching that resulted in microroughness with Sa values of 2.2–2.8 µm.

Surgical Procedure

The animals were preanesthetized with acepromazine 0.2%–1.5 mg/kg 10 minutes before administrating butorphanol (0.2 mg/kg) and medetomidine (7 µg/kg). The mixture was injected intramuscularly in the femoral quadriceps. The animals were then taken to the operating theater where, at the earliest opportunity, an intravenous catheter was inserted (diameter 22 or 20 G) into the cephalic vein, and propofol was infused at the rate of 0.4 mg/kg/min as a slow constant rate infusion. Conventional dental infiltration anesthesia was administered at the surgical sites. These procedures were carried out under the supervision of a veterinary surgeon.

Mandibular premolar extractions (${}_2P_{2,}\ {}_3P_{3,}\ {}_4P_4$) were carried out in the hemi-arches of each dog. The teeth were sectioned in a buccolingual direction at the bifurcation using a tungsten-carbide bur so that the roots could be individually extracted using a periotome and forceps without damaging the bony walls.

The apical portion of the socket was prepared using a 2 mm diameter pilot drill at 1,200 rpm under saline irrigation. Then, slow-speed sequential drilling with burs of 2.5 mm and 3.0 mm was performed at 800 rpm under saline irrigation. Randomly, three dual acid-etched implants and three dual acid-etched and sand-blasted implants were placed in the distal sockets of each mandible. Implant position was in relation to both (buccal and lingual) crestal wall heights. Subsequently, covering screws were adjusted in order to allow a submerged healing protocol. No grafting materials were used in the gaps between buccal plates and implants.

During the first week after surgery, the animals received the antibiotics and analgesics amoxicillin (500 mg, twice daily) and ibuprofen 600 mg (three times a day) via the systemic route. Sutures were removed after 2 weeks. The dogs were fed a soft-pellet diet for 14 days after the sutures were removed. Healing was evaluated weekly, and plaque control was maintained by flushing the oral cavity with clorhexidine digluconate.

Histological and Histomorphometric Analysis

Three animals were sacrificed at 4 weeks ($n = 3$) and the other three at 8 weeks ($n = 3$) following the implant procedure by means of an overdose of Pentothal Natrium (Abbott Laboratories, Madrid, Spain) and perfused through the carotid arteries with a fixative containing a mixture of 5% glutaraldehyde and 4% formaldehyde.

After sacrifice, the mandibles were retrieved by sharp dissection, soft tissue was removed by surgical blades, and initial clinical evaluation was performed to determine implant stability. If an implant was clinically unstable, it was excluded from the study.

For biomechanical testing, the bone blocks with implants were adapted to an electronic torque machine equipped with a 200 N/cm torque load cell (Test Resources, Minneapolis, MN, USA). Custom-machined tooling was adapted to the implants' hexagons, and the retrieved bone was carefully positioned to minimize angulation during testing. The implants were torqued to the point of interfacial fracture at a rate of ~0.19618 radians/s, and a torque versus displacement curve was recorded for each specimen. The torque machine was set to automatically stop when a torque drop of 10% from the highest load was detected. The rationale for this procedure was to minimize interface damage prior to histological procedures.[19–22]

After biomechanical testing, the bone blocks were kept in 10% buffered formalin solution for 24 hours, washed in running water for 24 hours, and gradually dehydrated in a series of alcohol solutions ranging from 70% to 100% ethanol. Once dehydrated, the samples were embedded in a methacrylate-based resin (Technovit 9100; Heraeus Kulzer, Wehrheim, Germany) according to the manufacturer's instructions. The blocks were then cut into slices (~300 μm thickness), aiming at the center of the implant along its long axis with a precision diamond saw (Isomet 2000; Buehler, Lake Bluff, IL, USA), and glued to acrylic plates with an acrylate-based cement, and a 24-hour setting time was allowed before grinding and polishing. The sections were then reduced to a final thickness of ~30 μm using a series of SiC abrasive papers (400, 600, 800, 1200, and 2400) (Buehler) in a grinding/polishing machine (Metaserv 3000; Buehler) under water irrigation. The sections were stained with toluidine blue and then evaluated by optical microscopy. The histological features were evaluated at ×50–200 magnification (Leica DM2500M; Leica Microsystems, Wetzlar, Germany).

Preliminary statistical analyses showed no effect of implant site on torque values (i.e., there were no consistent effects of positions ${}_2P_2$, ${}_3P_3$, ${}_4P_4$). Therefore, implant location was not taken into further consideration. Further statistical evaluation of torque measurement first used a mixed-model analysis of variance with one between-subjects factor (four levels of implant design and surfaces) and a random intercept to model potential dependencies arising from repeated observations within the same animal. Analysis showed that the random intercept term was unnecessary, and final analyses did not include a random intercept term. Statistical significance was indicated by p levels < 5%, and post hoc testing used the Fisher least significant difference test.

RESULTS

No complications affecting procedural conditions, postoperative infection, or other clinical concerns were experienced during either surgery or the follow-up period. No implants were excluded from the study due to clinical instability immediately after euthanization.

The torque to interface fracture results (Table 1) showed significant differences among the surface treatments ($p < .001$). The mean torque to interface fracture of the T DAE surface was 19.2 N/cm, and post hoc testing indicated that there was no statistical change from this level in the T DAE SB (23.07 N/cm) and the C DAE (27.4 N/cm) surfaces.

However, torque to failure increased significantly with the C DAE SB (49.22 N/cm) surface compared with all other groups ($p < .05$; see Table 1). Moreover, the C DAE surface showed higher bone biomechanical fixation when compared with the T DAE surface.

The T DAE SB surface showed higher torque to failure values in all the samples when compared with the T DAE surface.

There was no apparent effect of sacrifice time ($p > .32$) on measures of torque to failure.

The nondecalcified sample processing after controlled torque testing showed intimate bone contact with all implant surfaces at regions of cortical and trabecular bone. Higher magnification of the bone-to-implant interface region showed that the nondecalcified sections obtained after biomechanical testing presented minimal morphologic distortion because of bone disruption resulting from mechanical testing (Figures 2–5).

The wound healing pattern between the implant threads observed for all groups followed the intramembranous-type healing mode (see Figures 2–5), and appositional bone healing was observed at the implant surface whenever direct contact existed between implant and bone immediately following placement (see Figure 2A). In general, the healing chambers were filled with woven bone at 4 weeks, and bone microstructural evolution with onset of remodeling could be seen for all groups at 8 weeks (evidenced by the lighter staining at regions of lamellar bone replacing the darker stained woven bone between threads). However, temporal morphologic differences were observed between surface groups.

At 4 weeks for the T DAE surface group, woven bone formation occurred primarily in the central region of healing chambers (see Figure 2A), whereas for all other groups, woven bone formation occurred at both central regions and regions in close proximity to the implant surface (see Figures 3A, 4A, and 5A). Furthermore, whereas multiple primary osteonic structures were observed for the T DAE SB, C DAE, and C DAE SB

TABLE 1 GLM Analysis of Variance Statistical Summary

Source	Numerator df	Denominator df	F	Significance
Intercept	1	35	422.85	.000
Time in vivo	1	35	0.989	.327
Surface	3	35	20.729	.000
Time in vivo X Surface	3	35	0.128	.943

Surface	Mean	SEM	df	95% CI Lower Bound	95% CI Upper Bound
T DAE	19.2[b]	2.858	35	13.39	25.00
T DAE SB	23.07[b]	2.858	35	17.27	28.88
C DAE	27.4[b]	2.858	35	21.58	33.19
C DAE SB	49.22[a]	2.858	35	43.15	55.28

The different letters represent statistically homogenous groups.
C DAE = cylindrical double acid etched; C DAE SB = cylindrical double acid etched/sandblasted; CI = confidence interval; df = degrees of freedom; SEM = standard error of the mean; T DAE, tapered double acid etched; T DAE SB, tapered double acid etched/sandblasted.

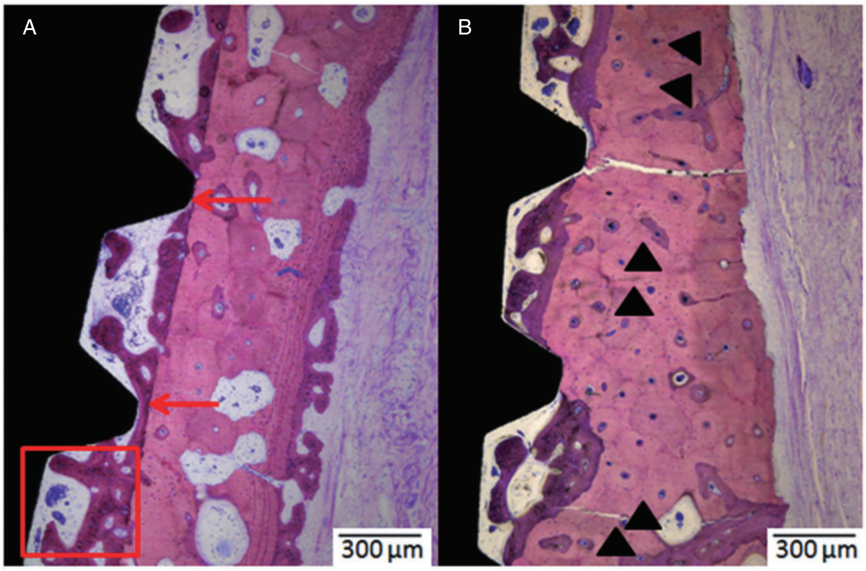

Figure 2 Optical micrographs obtained at ×40 original magnification of the T DAE group at 4 weeks (A) and 8 weeks (B) implantation time. Note the presence of woven bone formation as early as 4 weeks in vivo through the intramembranous-like pathway in the healing chamber region (*box*), and the appositional healing taking place at the threads that were in intimate contact with the osteotomy wall immediately after placement (*arrows*). A slight bone microstructural evolution was observed at 8 weeks, where primary osteonic structures indicating the onset of remodeling after the initial modeling healing stage were observed (*arrowheads*). Toluidine blue stain. T DAE = tapered with dual acid etched.

surfaces at 4 weeks, this structural bone feature was seldom observed in the T DAE group.

At 8 weeks, replacement of woven bone by lamellar bone was observed for all groups (see Figures 2B, 3B, 4B, and 5B). No qualitative morphologic differences were observed among the different implant surface groups at 8 weeks. However, remodeling occurred in regions where woven bone was distributed within the healing chambers at 4 weeks for the different groups, where the C DAE and C DAE SB groups presented

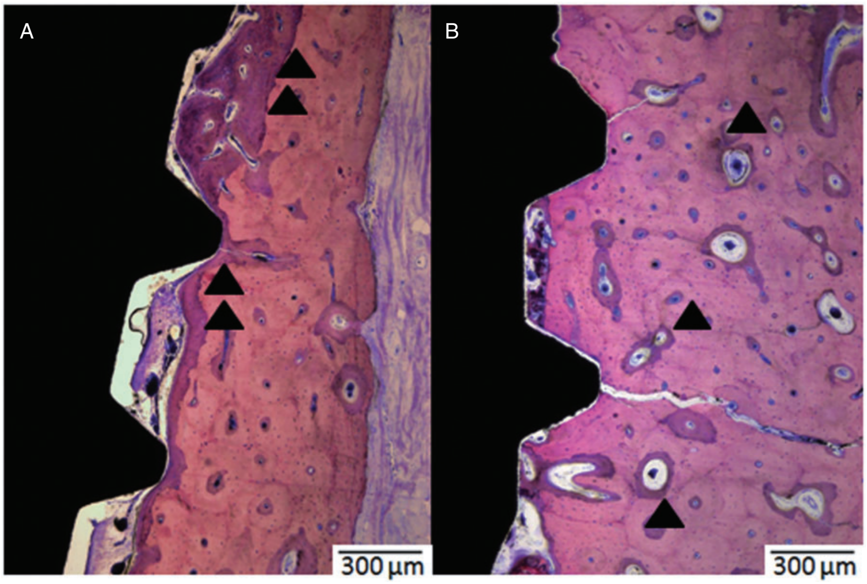

Figure 3 Optical micrographs obtained at ×40 original magnification of the T DAE SB group at 4 weeks (A) and 8 weeks (B) implantation time. Note the presence of multiple primary osteonic structures indicating the onset of remodeling following the initial modeling healing stage as early as 4 weeks implantation time (*arrowheads*). Toluidine blue stain. T DAE SB = tapered with dual acid etched and sandblasted.

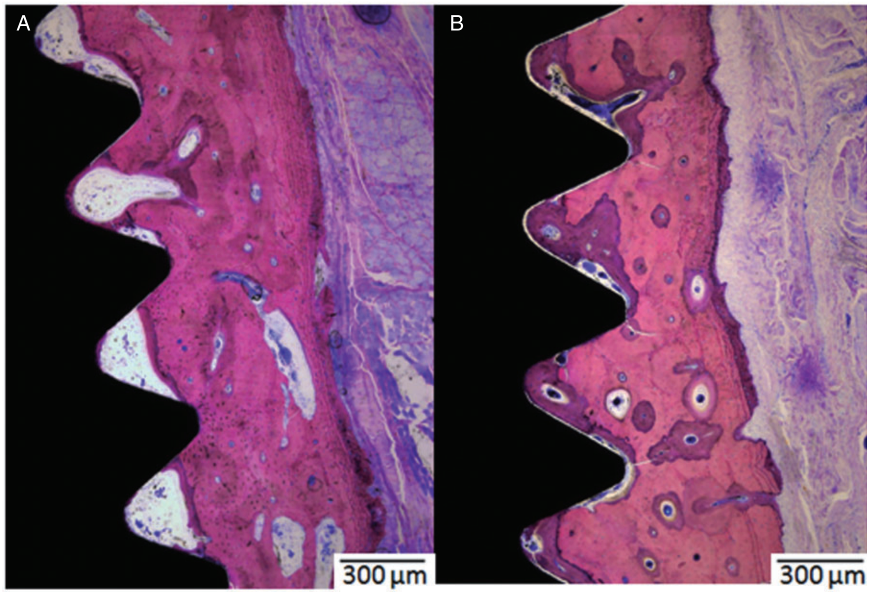

Figure 4 Optical micrographs obtained at ×40 original magnification of the C DAE group at 4 weeks (A) and 8 weeks (B) implantation time, where woven bone formation occurred at both central regions and regions in close proximity to the implant surface. Toluidine blue stain. C DAE = cylindrical with dual acid etched.

woven bone replacement at both central regions and regions in close proximity with the implant surface (see Figures 4B and 5B) and the T DAE and T DAE SB groups showed woven bone replacement at the central region of the healing chamber only (see Figures 2B and 3B).

DISCUSSION

Although a large database addressing the bone healing around screw-type implants is available, a substantially smaller body of literature has focused on endosseous implant design whereby spaces between the implant

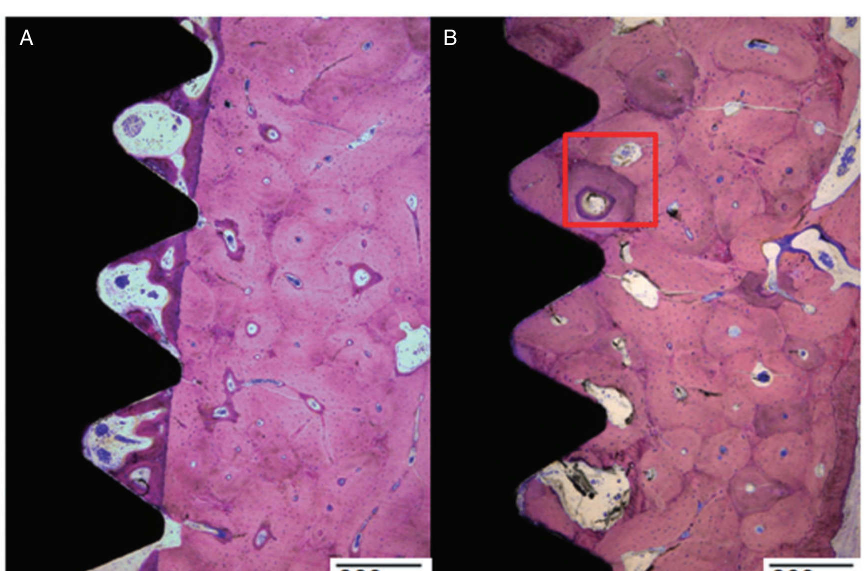

Figure 5 Optical micrographs obtained at ×40 original magnification of the C DAE SB group at 4 weeks (A) and 8 weeks (B) implantation time. Note the remarkable amount of remodeling evidenced by the lighter staining at 8 weeks (*box*), showing rapid replacement of woven bone (dark blue) by lamellar bone throughout the healing chamber. Toluidine blue stain. C DAE SB = cylindrical with dual acid etched and sandblasted.

inner diameter and osteotomy walls develop into healing chambers.[7,9]

The bone around screw root form implants, where the intimate contact between the osteotomy wall and the implant surface results in high degrees of primary stability, undergoes localized bone necrosis near the implant surface before bone apposition ensures its biomechanical fixation.[7,9] Healing chambers provide little primary stability but have been shown to fill rapidly with woven bone, filling the entire volume occupied by blood clots following placement, and so achieving osseointegration.[7,9,27–29] Thus, changes in surface texture and chemistry are likely to change the bone healing kinetics at the thread region during the early stages following implantation.

Over the years, endosseous implant surfaces have evolved from as-machined to the more osteoconductive moderately rough surfaces in common use today.[3,4,10,11,16,28] Highly osteoconductive PSHA-coated implants were also introduced but fell from favor in clinical practice owing to the potential development of a weak interface between coating and implant substrate.[4,6,8] In an attempt to benefit from both the surface roughness presented by moderately rough surfaces and chemistry similar to that of PSHA-coated implants, bioceramics have been incorporated in smaller domains.[4,12,17,19–22,28] The present study evaluated the early host response to two different commercially available implant surfaces in tapered and cylindrical screw root form implants.

Although the literature asserts that titanium oxides are present on acid-etched surfaces and that these present a smooth roughness profile,[10] atomic force microscopy-based texture analysis of the double acid-etched and sandblasted surface[19] investigated in the present study found significantly higher Sa values in both the tapered and cylindrical design.

Our results showed that the C DAE SB implants presented significantly higher torque to interface fracture values than T DAE, T DAE SB, and C DAE, indicating that the thread design and surface structure played a significant role in their biomechanical fixation during early stages following implantation.

The low degree of mechanical disruption between bone and implant observed in the histology slides following mechanical testing was probably because of implant shape combined with proper specimen alignment and the slow torque rate applied. The implant's geometric configuration allowed free rotation under torque and precise stopping of the machine when it registered a 10% drop from the maximum load recorded.[19,21,22] In this way, mechanical disruption was observed in only a few histological sections[19,21,22] and this did not compromise qualitative histomorphologic evaluations. Even though removal torque tests showed higher scores for implants with double acid-etched and sandblasted (DAE SB) surfaces than double acid etched (DAE) ones, removal of implants with these rough surfaces frequently resulted in fractures within the bone distant from the implant surface, suggesting the existence of an implant-to-bone "bond."

Thread depth, thread thickness, thread face angle, and thread pitch are some of the varying geometric patterns that determine the functional thread surface affecting woven bone formation throughout the volume occupied by the blood clot immediately after placement.

General observation of the histological sections showed that the specimens from any group showed intimate bone-to-implant contact irrespective of the implant surface, demonstrating that all surfaces were biocompatible and osteoconductive. Furthermore, regardless of surface modification, the wound healing sequence and mode observed in the present study was similar to that described in earlier studies for healing chamber models[7,9,27] in which osseointegration was successfully established in implants presenting large contact-free surfaces. However, qualitative histomorphologic evaluation showed a more even distribution of woven bone (at both central and peripheral regions of the threads) for the DAE SB surfaces compared with the DAE surface. It might be that this was due to the DAE's decreased ability to retain the blood clot uniformly over time in comparison with the DAE SB surface[10] and to the different thread geometry, which might have altered the bone location and healing kinetics within the chamber.

Thread configuration is an important factor for biomechanical optimization of dental implant design. Threads are used to maximize initial contact, improve initial stability, enlarge implant surface area, and favor dissipation of interfacial stress. Thread depth, thread thickness, thread face angle, and thread pitch are some of the varying geometric patterns that determine the functional thread surface and could affect woven bone formation. For these thread parameters, thread pitch shows more operative significance, which in turn might affect new bone apposition.

The large number of studies reporting the benefits of surface topographic and chemical modifications around screw type implants, together with an increasing body of literature depicting the benefits of surface modification in endosseous implants presenting healing chambers demonstrate that surface modifications should be taken into account by clinicians whenever early implant loading is an option. However, the question of whether the same surface modification to implants of different design will result in faster bone response and/or biomechanical stabilization either with or without healing chambers and the question of how the different factors may be combined for optimum performance warrant further investigation.

CONCLUSIONS

The DAE SB surface treatment positively influenced the early bone biomechanical fixation of tapered and cylindrical screw root form implants. However, the addition of sandblasting was not seen to increase values for T DAE SB, suggesting that the higher values seen in C DAE SB were not due simply to sandblasting; further research is required to explore how the combinations of surface treatment and root form work to optimize biomechanical fixation. Furthermore, the cylindrical implant provided increased mechanical properties. Both thread design and surface structure played a significant role in the biomechanical fixation and bone formation during early stages following implantation.

REFERENCES

1. Chuang SK, Tian L, Wei LJ, Dodson TB. Kaplan-Meier analysis of dental implant survival: a strategy for estimating survival with clustered observations. J Dent Res 2001; 80:2016–2020.
2. Chuang SK, Tian L, Wei LJ, Dodson TB. Predicting dental implant survival by use of the marginal approach of the semiparametric survival methods for clustered observations. J Dent Res 2002; 81:851–855.
3. Albrektsson T, Wennerberg A. Oral implant surfaces: part 2 – review focusing on clinical knowledge of different surfaces. Int J Prosthodont 2004; 17:544–564.
4. Coelho PG, Granjeiro JM, Romanos GE, et al. Basic research methods and current trends of dental implant surfaces. J Biomed Mater Res B Appl Biomater 2009; 88:579–596.
5. Bottino MC, Coelho PG, Henriques VA, Higa OZ, Bressiani AH, Bressiani JC. Processing, characterization, and in vitro/in vivo evaluations of powder metallurgy processed Ti-13Nb-13Zr alloys. J Biomed Mater Res A 2009; 88:689–696.
6. Lemons J, Dietch-Misch F. Biomaterials for dental implants. In: Misch CE, ed. Contemporary implant dentistry. St. Louis: Mosby, 1999:271–302.
7. Berglundh T, Abrahamsson I, Lang NP, Lindhe J. De novo alveolar bone formation adjacent to endosseous implants. Clin Oral Implants Res 2003; 14:251–262.
8. Lemons JE. Biomaterials, biomechanics, tissue healing, and immediate-function dental implants. J Oral Implantol 2004; 30:318–324.
9. Leonard G, Coelho P, Polyzois I, Stassen L, Claffey N. A study of the bone healing kinetics of plateau versus screw root design titanium dental implants. Clin Oral Implants Res 2009; 20:232–239.
10. Albrektsson T, Wennerberg A. Oral implant surfaces: part 1 – review focusing on topographic and chemical properties of different surfaces and in vivo responses to them. Int J Prosthodont 2004; 17:536–543.
11. Calvo-Guirado JL, Ortiz-Ruiz AJ, Negri B, López-Marí L, Rodríguez-Barba C, Schlottig F. Histological and histomorphometric evaluation of immediate implant placement on a dog model with a new implant surface treatment. Clin Oral Implants Res 2010; 21:308–315.
12. Marin C, Granato R, Suzuki M, Gil JN, Piattelli A, Coelho PG. Removal torque and histomorphometric evaluation of bioceramic grit-blasted/acid-etched and dual acid-etched implant surfaces: an experimental study in dogs. J Periodontol 2008; 79:1942–1949.
13. Negri B, Calvo-Guirado JL, Ramírez-Fernández MP, Maté Sánchez-de Val J, Guardia J, Muñoz-Guzón F. Peri-implant bone reactions to immediate implants placed at different levels in relation to crestal bone. Part II: a pilot study in dogs. Clin Oral Implants Res 2011. DOI: 10.1111/j.1600-0501.2011.02290.x [Epub ahead of print].
14. Davies JE. Understanding peri-implant endosseous healing. J Dent Educ 2003; 67:932–949.
15. Eraslan O, Inan O. The effect of thread design on stress distribution in a solid screw implant: a 3D finite element analysis. Clin Oral Investig 2010; 14:411–416.
16. Butz F, Aita H, Wang CJ, Ogawa T. Harder and stiffer bone osseointegrated to roughened titanium. J Dent Res 2006; 85:560–565.
17. Ogawa T, Ozawa S, Shih JH, et al. Biomechanical evaluation of osseous implants having different surface topographies in rats. J Dent Res 2000; 79:1857–1863.
18. Yang Y, Kim KH, Ong JL. A review on calcium phosphate coatings produced using a sputtering process – an alternative to plasma spraying. Biomaterials 2005; 26:327–337.
19. Coelho PG, Lemons JE. Physico/chemical characterization and in vivo evaluation of nanothickness bioceramic depositions on alumina-blasted/acid-etched Ti-6Al-4V implant surfaces. J Biomed Mater Res A 2008; 90:351–361.
20. Coelho PG, Cardaropoli G, Suzuki M, Lemons JE. Histomorphometric evaluation of a nanothickness bioceramic

deposition on endosseous implants: a study in dogs. Clin Implant Dent Relat Res 2009; 11:292–302.

21. Coelho PG, Cardaropoli G, Suzuki M, Lemons JE. Early healing of nanothickness bioceramic coatings on dental implants. An experimental study in dogs. J Biomed Mater Res B Appl Biomater 2009; 88:387–393.
22. Granato R, Marin C, Suzuki M, Gil JN, Janal MN, Coelho PG. Biomechanical and histomorphometric evaluation of a thin ion beam bioceramic deposition on plateau root form implants: an experimental study in dogs. J Biomed Mater Res B Appl Biomater 2009; 90:396–403.
23. Mendes VC, Moineddin R, Davies JE. Discrete calcium phosphate nanocrystalline deposition enhances osteoconduction on titanium-based implant surfaces. J Biomed Mater Res A 2009; 90:577–585.
24. Orsini G, Piatelli M, Scarano A, et al. Randomized, controlled histologic and histomorphometeric evaluation of implants with nanometer-scale calcium phosphate added to the dual acid-etched surface in the human posterior maxilla. J Periodontol 2006; 77:1984–1990.
25. Park YS, Yi KY, Lee IS, Han CH, Jung YC. The effects of ion beam-assisted deposition of hydroxyapatite on the grit-blasted surface of endosseous implants in rabbit tibiae. Int J Oral Maxillofac Implants 2005; 20:31–38.
26. Suzuki K, Aoki K, Ohya K. Effects of surface roughness of titanium implants on bone remodeling activity of femur in rabbits. Bone 1997; 21:507–514.
27. Coelho PG, Suzuki M, Guimaraes MV, et al. Early bone healing around different implant bulk designs and surgical techniques: a study in dogs. Clin Implant Dent Relat Res 2010; 12:202–208.
28. Mendes VC, Moineddin R, Davies JE. The effect of discrete calcium phosphate nanocrystals on bone-bonding to titanium surfaces. Biomaterials 2007; 28:4748–4755.
29. Negri B, Calvo-Guirado JL, Zamora GP, Ramírez Fernández MP, Delgado Ruíz R, Muñóz Guzón F. Peri-implant bone reactions to immediate implants placed at different levels in relation to crestal bone. Part I: a pilot study in dogs. Clin Oral Implants Res 2011. DOI: 10.1111/j.1600-0501.2011.02158.x [Epub ahead of print].